Science of the Total Environment 827 (2022) 154155

Contents lists available at ScienceDirect

Science of the Total Environment

journal homepage: www.elsevier.com/locate/scitotenv

Arsenic speciation analysis in porewater by a novel colorimetric assay

Andrea Castillejos Sepúlveda [a,*], Lais M. Gatti [a], Carolin F. Kerl [b], Arjun Chennu [c], Judith M. Klatt [a,*]

[a] Microsensor Group, Max Planck Institute for Marine Microbiology, Bremen, Germany
[b] Environmental Geochemistry, Bayreuth Center for Ecology and Environmental Research (BayCEER), University of Bayreuth, D-95440 Bayreuth, Germany
[c] Data Science and Technology, Leibniz Centre for Tropical Marine Research, Bremen, Germany

HIGHLIGHTS

- New field usable colorimetric method measures arsenate, arsenite and phosphate.
- The concentration ranges are ~5–40 μM and ~ 0.1–15 μM in low sample volume (100 μL).
- Depth profiles of arsenate and arsenite can rapidly be obtained from porewater.
- Microbial iron and arsenic cycling may release arsenic from the soil of a brook.
- Downstream soil retains arsenic and prevents contamination of adjacent rivers.

GRAPHICAL ABSTRACT

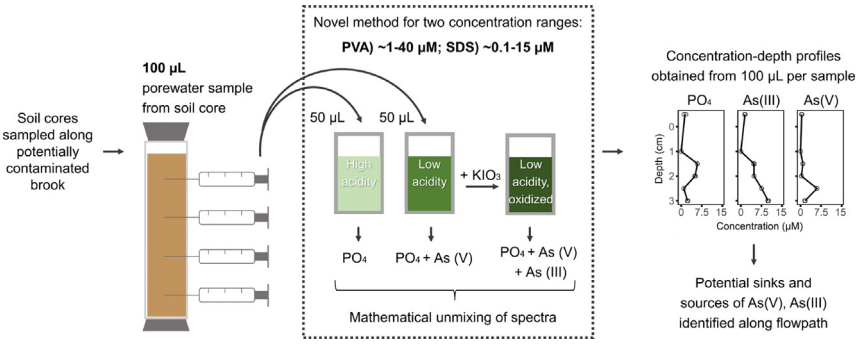

ARTICLE INFO

Article history:
Received 26 November 2021
Received in revised form 22 February 2022
Accepted 22 February 2022
Available online 26 February 2022

Editor: Mae Sexauer Gustin

Keywords:
Arsenate
Arsenite
Arsenic speciation
Soil
Dissolved inorganic arsenic
Porewater

ABSTRACT

Arsenic is common toxic contaminant, but tracking its mobility through submerged soils is difficult because microscale processes dictate its speciation and affinity to minerals. Analyses on environmental dissolved arsenic (As) species such as arsenate and arsenite currently require highly specialized equipment and large sample volumes. In an effort to unravel arsenic dynamics in sedimentary porewater, a novel, highly sensitive, and field-usable colorimetric assay requiring 100 μL of sample was developed. Two complementary protocols are presented, suitable for sub-micromolar and micromolar ranges. Phosphate is a main interfering substance, but can be separated by measuring phosphate and arsenate under two different acidities. Arsenite is assessed by oxidation of arsenite to arsenate in the low-acidity reagent. Optimization of the protocol and spectral analyses resulted in elimination of various interferences (silicate, iron, sulfide, sulfate), and the assay is applicable across a wide range of salinities and porewater compositions. The new assay was used to study As mobilization processes through the soil of a contaminated brook. Water column sources of arsenic were limited to a modest input by a groundwater source along the flow path. In one of the sites, the arsenite and arsenate porewater profiles showed active iron-driven As redox cycling in the soil, which may play a role in arsenic mobilization and releases arsenite and arsenate into the brook water column. Low arsenic concentrations downstream from the source sites indicated arsenic retention by soil and dilution with additional sources of water. Arsenic is thus retained by the Bossegraben before it merges with larger rivers.

1. Introduction

To understand biogeochemical processes in benthic or soil systems, determining the depth distribution of soluble reactive species is key. The sediment- and soil-associated cycling of various arsenic (As) species is of great interest due to their short- and long-term effects on human and ecosystem health. Elevated levels of As, above the recommended 10 μg/L (133 nM) for drinking water (WHO, 2017), can be found in a wide variety of environments, and are usually associated to mountain ranges of volcanic origin (Mukherjee et al., 2019; Tapia et al., 2019), with mining activity

* Corresponding authors.
E-mail addresses: acastill@mpi-bremen.de (A. Castillejos Sepúlveda), jklatt@mpi-bremen.de (J.M. Klatt).

http://dx.doi.org/10.1016/j.scitotenv.2022.154155

boosting the release of As into groundwater (Nickson et al., 1998; Rodriǵuez-Lado et al., 2013), and adjacent the soil and sediment. Especially in crop fields and peat bogs with high particulate and dissolved organic matter, As tends to accumulate (Kuramata et al., 2011; Thomas Arrigo et al., 2016).

Inorganic As mainly occurs in environmental samples as arsenite (AsO_3^{3-}) or arsenate (AsO_4^{3-}) (Oremland and Stolz, 2003), here referred to as "As(III)" and "As(V)", respectively. The species differ in their mobility and toxicity. Redox cycling in ecosystems is complex due to its dependence on many environmental factors, and has therefore been understudied (Oremland and Stolz, 2003). Redox transformations of As can be abiotic or microbially mediated. The genetic repertoire for both As(III) oxidation and As(V) reduction is widespread across the phylogenetic tree, and an important role of As cycling in the early Earth has been suggested (Wells et al., 2020). Even today in environments with low concentrations, such as oxygen-deficient ocean zones, rates of microbial As cycling may be high (Saunders et al., 2019). However, assessing the availability of the As species for microbial and abiotic transformations is not trivial, especially in sediments and soils. This is because availability is influenced by precipitation, dissolution, and binding of As to various minerals, which are influenced by its redox state, pH, and the species of minerals in the surrounding sediment (Dixit and Hering, 2003). This hinders the understanding of mechanisms behind the mobility of As, which would be crucial towards minimizing exposure and harm to humans. Fine scale determination of As speciation may help unravel patterns of dissolution and precipitation which would be otherwise overlooked (Hossain et al., 2012; Smedley and Kinniburgh, 2002). Samples such as porewater extracted from soil can provide information on a mm to cm-scale but are only feasible with analysis tools for low sample volume (<2 mL usually). Thus, sensitive, yet simple and field usable, methods capable of quantifying As concentration and speciation in low sample volumes are necessary.

1.1. Development of a novel colorimetric analysis for arsenic in natural ecosystems

Concern about As contamination around the world has stimulated the development of a variety of methods to measure As concentrations in bulk samples of water to assess water potability. A variety of methods exist for As analysis in drinking water. Accurate determination of the concentration and speciation of As in environmental water samples requires specialized laboratory instrumentation such as atomic absorption spectroscopy (AAS), atomic fluorescence spectroscopy (AFS), and inductively coupled plasma mass spectroscopy (ICP-MS); speciation analyses require further coupling to an IC or HPLC. For field measurements, researchers have to rely on alternate methods, such as kits, cartridges, and colorimetric methods.

The commonly used commercial field kits, based on the Gutzeit method (Sanger and Black, 1907), only measure total As. Since the adsorption of As onto minerals strongly depends on speciation, these kits are not very useful for studies towards mobility and bioavailability. Additionally, the kits are not reliable to determine if water is safe for consumption according to the WHO guidelines - despite extensive attempts for improvement (Barnes and Murray, 1930; Goldstone, 1946; Kearns et al., 2019).

On-site determination of the speciation of As in water is even more challenging. Usually, water is first filtered through solid-phase extraction cartridges that selectively absorb a given As species (Le et al., 2000; Gómez et al., 1997; Bednar et al., 2002). Such methods require large sample volumes (15–50 mL) and further processing by AAS or ICP-MS. Therefore, most current assays and commercial kits are unsuitable for the small sample volumes that can be obtained from sediments.

Colorimetric methods have been developed as a low-cost alternative to obtain rapid information about As concentration and speciation from sediment and water samples (Hu et al., 2012; Lenoble et al., 2003). Many of these assays take advantage of the molybdenum blue method for phosphate (PO_4^{3-}) (Murphy and Riley, 1962) that is also sensitive to As(V). However, the applicability, feasibility, and detection limit of these assays in low sample volumes and complex sample matrices is limited. Building on these assays, we therefore aimed to develop a sensitive and field-usable colorimetric method for determination with high specificity of As concentrations and redox speciation in small (100 μL) samples with high levels of potentially interfering solutes. The method was used to study As cycling in soil porewater along the flow path of an arsenic-contaminated brook.

1.2. Arsenic contamination from mining deposit runoff

Mining deposits and mining waste form a major source of contamination by leaching of As (Bundschuh et al., 2012; Tapia et al., 2019; Williams, 2001). Mining in the Harz mountains, Germany, for instance, has taken place since the Middle Ages, with ensuing polluting deposits (Deicke and Ruppert, 2013). Pollution from the larger area has been shown to have wide-reaching effects due to the intersection of multiple rivers and artificial canals. According to Richter (2018), As from around Friedeburgerhütte (~100 km east of Oker) was detected as far as Hamburg, over 200 km north of the mining region. Local Harz As contamination dramatically worsened upon the import and processing of As-containing ores, even in the Northern Harz region that is characterized by low natural As abundance. In the mid-20th century, a deposit located near Oker has been used for such As-rich waste. The deposit was later sealed to prevent further leaching of As (Fachbereich Bauen & Umwelt - Bodenschutz / Deponiemanagement and Fachbereich Umwelt und Gewässerschutz, Landkreis Goslar, personal communication, 2021). We hypothesized that the Bossegraben, a brook flowing along the deposit periphery, is still impacted by As locally leaching from the deposit and from previously deposited iron-bound As in the brook's soil. The aims of this study were therefore to characterize the input of dissolved As into the brook's water column and to assess if the soil acts a source or sink of As along the flow path of the Bossegraben, using the newly developed speciation analysis for porewater.

2. Materials and methods

2.1. Principles

2.1.1. Chemistry

The classic molybdenum blue method for PO_4^{3-} detection was adapted and modified to achieve a low limit of detection for As, and As speciation, in low sample volumes, as well as to correct for interference of PO_4^{3-}. In the novel method presented here, a porewater sample is split into 2 subsamples (Fig. 1B). One subsample is treated with low acidity, while the other is treated with high acidity. Both low- and high- acidity reagents have molybdate and malachite green. Phosphate forms a colorless to pale yellow complex with molybdate (*phosphomolybdic acid* or *molybdophosphoric acid*), which is further treated to yield a stable colorful product by dyeing with malachite green (Altmann et al., 1971; Carter and Karl, 1982; Singh and Shukla, 2003). Due to its structural similarity to PO_4^{3-}, As(V) also forms a complex with molybdate (Blomqvist et al., 1993; Huang and Zhang, 2006; Linge and Oldham, 2001; Pett, 1933). Although the exact chemical reaction remains unclear (Nagul et al., 2015), it is likely similar to

$$As(V) + (NH_4)_6Mo_7O_{24} \xrightarrow{H_2SO_4,\text{malachite green}} H_3AsMo_{12}O_{40} - \text{malachite green} \quad (1)$$

$$PO_4^{3-} + (NH_4)_6Mo_7O_{24} \xrightarrow{H_2SO_4,\text{malachite green}} H_3AsMo_{12}O_{40} - \text{malachite green} \quad (2)$$

Eqs. (1) and (2) are dependent on acidity: complexation of only As(V) with molybdate is inhibited in high acidity, but not in low acidity. This is the greatest difference from previous methods, which removed As(V) interference by reduction to As(III), usually by a hazardous and inefficient chemical reaction (Supp. Materials and Methods 1.1.2).

Arsenite does not form a complex with molybdate due to the difference in shape and charge. Therefore, the sample treated with low acidity is eventually also oxidized (Fig. 1C), allowing for the measurement of As(III) converted into As(V).

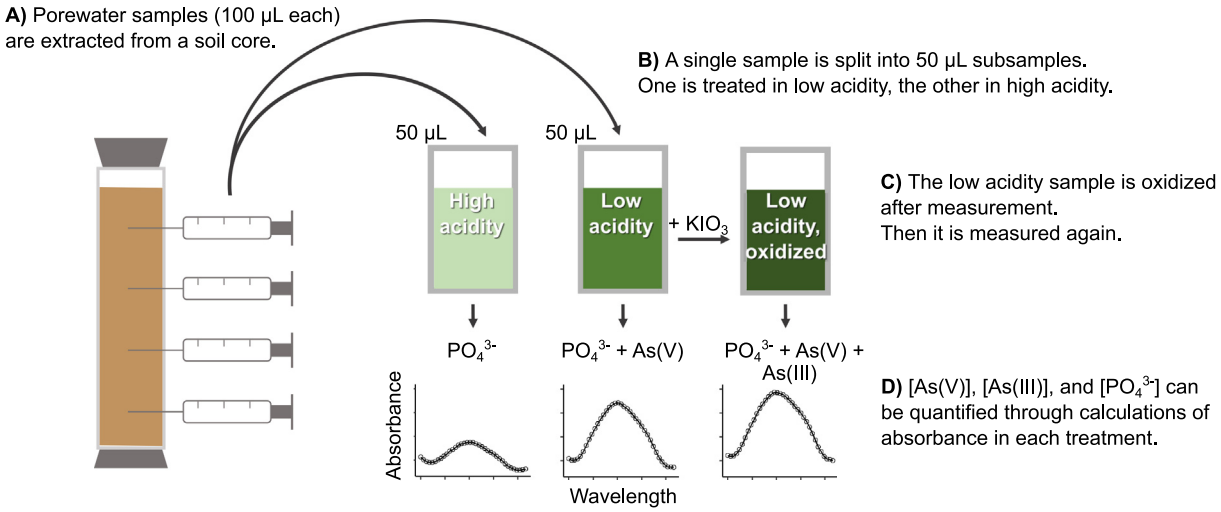

Fig. 1. Schematic representation of the workflow of a novel colorimetric method for the measurement of As(V) and As(III) in porewater samples.

After reacting with malachite green, the complexes exhibit a wide absorbance peak, with two maxima at ~600 and ~ 650 nm (Supp. Fig. S1). The spectral shape depends on the analytes, their concentration, the sample matrix and the age of the reagents. Thus, calibrations in an adequate matrix must be made for each sample set on the same day.

2.1.2. Calculation

From the differences in absorbance of the three reaction mixtures, the concentrations of PO_4^{3-}, As(III) and As(V) are calculated by considering a set of three linear equations. To arrive at this set, regression coefficients (slopes and intercepts) of the absorbance index (AI) with respect to the concentration of each analyte in each reagent mixture are obtained using standards (i.e., the calibration data is fitted by linear regression). AI is chosen based on the target analyte concentration range (Fig. 2). In the high acidity reagent (subscript H), regression equations are obtained for As(V) and PO_4^{3-} as

$$AI_H\left(PO_4^{3-}\right) = \gamma_H\left[PO_4^{3-}\right] + \delta_H \text{ and} \quad (3)$$

$$AI_H(As(V)) = \alpha_H \times [As(V)] + \beta_H, \quad (4)$$

where regression coefficients are defined as follows: γ is the slope and δ is the y-intercept of PO_4^{3-}, α is the slope and β is the y-intercept of As(V). Due to the acidity-based inhibition of complex formation with As(V), $\alpha_H << \gamma_H$ or α_H is negligible. In the low acidity reagent (subscript L) regression equation for all three analytes are obtained as

$$AI_L\left(PO_4^{3-}\right) = \gamma_L \times \left[PO_4^{3-}\right] + \delta_L \quad (5)$$

$$AI_L(As(V)) = \alpha_L \times [As(V)] + \beta_L \text{ and} \quad (6)$$

$$AI_L(As(III)) = \varepsilon_L \times [As(III)] + \kappa_L \quad (7)$$

where ε and κ are the slope and y-intercept of As(III), respectively. Here, complex formation is not inhibited and the slopes α_L and γ_L have similar values, while ε_L is substantially smaller than the other slopes or negligible. The procedure is identical for the analytes in the oxidant supplemented reagent (subscript LO) and follows

$$AI_{LO}\left(PO_4^{3-}\right) = \gamma_{LO} \times \left[PO_4^{3-}\right] + \delta_{LO} \quad (8)$$

$$AI_{LO}(As(V)) = \alpha_{LO} \times [As(V)] + \beta_{LO} \text{ and} \quad (9)$$

$$AI_{LO}(As(III)) = \varepsilon_{LO} \times [As(III)] + \kappa_{LO} \quad (10)$$

where all slopes have similar values. This is because after oxidant is added to the sample previously treated with low acidity reagent, As(III) is oxidized to As(V), which may then complex with molybdate.

In mixed samples with multiple analytes, AI is expected to be the sum of their individual contribution. Under high acidity AI is dependent on the PO_4^{3-} concentration (the interfering background) and As(V) concentration according to.

$$AI_H = AI_H(As(V)) + AI_H\left(PO_4^{3-}\right) \quad (11)$$

The direct replacement with Eqs. (3)–(4), would introduce multiple intercepts into the equation, which leads to an overestimation of the contribution of each analyte. Therefore, first an average of the y-intercepts Φ is calculated as

$$\Phi_H = (\delta_L + \beta_H)/2 \quad (12)$$

and then the dependency of AI_H on PO_4^{3-} and As(V) is defined as

$$AI_H = \alpha_H \times [As(V)] + \gamma_H \times \left[PO_4^{3-}\right] + \Phi_H \quad (13)$$

In the low acidity and oxidant-supplemented subsamples AI_L and AI_{LO} will depend on all analytes, which yields the following equations:

$$AI_L = \alpha_L \times [As(V)] + \varepsilon_L \times [As(III)] + \gamma_L \times \left[PO_4^{3-}\right] + \Phi_L \quad (14)$$

$$AI_{LO} = \alpha_{LO} \times [As(V)] + \varepsilon_{LO} \times [As(III)] + \gamma_{LO} \times \left[PO_4^{3-}\right] + \Phi_{LO} \quad (15)$$

where Φ_L and Φ_{LO} are the average of the y-intercepts from Eqs. (5)–(7) and (8)–(10), respectively. Using all three absorbance readings, the three unknowns (As(III), As(V) and PO_4^{3-}) can be determined from the three Eqs. (13)–(15).

2.1.3. Optimization procedure

Sensitivity in the novel colorimetric assay was improved, compared to classical methods, by modification of the reagent mixture and through choice of spectral measurements. In the reagent mixture, sensitivity was enhanced by surfactant addition, as well as by using malachite green to dye the Mo-As(V) and Mo-PO_4^{3-} complexes, instead of the traditionally-used reduction with ascorbic acid (Supp. Figs. S2 & S3). A variety of spectral indices ("AI") were tested to optimize the limit of detection (LoD) across a wide range of analyte concentrations and their mixtures, as well as to minimize interference by PO_4^{3-} (details in Supp. Materials and Methods 1.1.3). A flowchart was devised to help navigate the choice of absorbance measurements (Fig. 2). An example of the usage of this flowchart can be found in

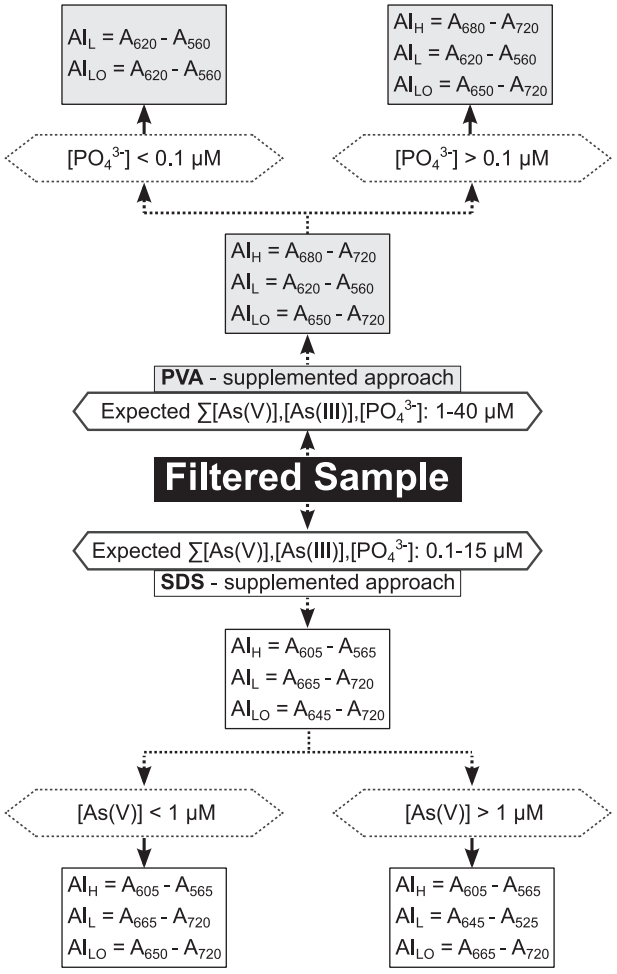

Fig. 2. Flowchart to aid in decision-making for finding suitable measurement parameters for samples in the range of 1–50 μM As(V), As(III) or PO_4^{3-} using the PVA-supplemented assay, and 0.1 to 15 μM As(V), As(III) or PO_4^{3-} using SDS-supplemented assay, beginning with "Filtered Sample". Absorbance Index (AI) values are calculated for each reagent through subtraction of absorbance (A) at one wavelength minus absorbance at another wavelength. Wavelengths in nanometers are specified as subscripts of A. Reagents are specified by subscripts of AI: low acidity (L), high acidity (H), oxidized low acidity (LO). AI_H, AI_L, and AI_{LO} may then be substituted into Eqs. (13)–(15) to solve for [As(V)], [As(III)], and [PO_4^{3-}]. Polygons represent decisions, which must be made by the user regarding analyte concentrations in a sample, rectangles represent systems of equations to be followed. Dotted arrows indicate that further calculations will be done, while solid arrows indicate a 'final' set of equations of a given sample. The subscripts under each Greek letter indicate the reagent in which the calibration curve was calculated. An example of flowchart use for analysis of an unknown sample can be found in Supp. to Materials and Methods (1.3).

the Supp. to Materials and Methods (1.2). Details of the optimization procedure are in the Supp. to Materials and Methods (1.4–1.5).

2.2. Experimental

All chemicals were obtained from Sigma Aldrich, with the exception of H_2SO_4 (Merck), iron (III) nitrate nonahydrate (Merck), artificial sea salt (Tropic Marin), and sodium metasilicate pentahydrate (Fluka). As(V) and As(III) standards used for ICP-MS analysis were obtained from Fluka.

2.2.1. Colorimetric assay

2.2.1.1. Standard preparation. Arsenate and phosphate calibration standards were prepared fresh from stocks of 10 mM. Daily, a calibration standard of 10 mM arsenite in Milli-Q was prepared from sodium (meta)arsenite. Arsenate stocks were prepared from sodium arsenate. Phosphate stocks were prepared from potassium phosphate monobasic.

Standards in the range of 0.1–50 μM were made with either ultrapure water (Milli-Q), or with artificial saltwater of 35 or 70 g/L, hereafter referred to as ASW and 2xASW.

2.2.1.2. Laboratory protocols for determination of As(V) and As(III) concentration in porewater. Two different assays were developed; they differ in sensitivity due to the use of different surfactants. The first assay depends on the addition of polyvinyl alcohol (**PVA**) as a surfactant, for samples with expected concentrations of 1–40 μM Σ([As(V)],[As(III)],[PO_4^{3-}]). The second uses sodium dodecyl sulfate (**SDS**) as the surfactant, for samples with expected concentrations of 0.1–15 μM Σ([As(V)],[As(III)],[PO_4^{3-}]). Both the PVA and SDS-supplemented assays follow the basic workflow in Fig. 1 and only differ in the specifics of the reagent mixture and spectral index choice. Including addition of samples to the plate and fresh reagent preparation, and reaction time, the total time necessary for each assay was around 7 h for 96 samples analyzed in 96-well plates. Separate "lab ready" step-by-step protocols for the assays and protocols for use of the assay in cuvettes are provided in the Supp. to Materials and Methods 1.2 and 1.4, respectively. Despite the number of steps in the workflow, the assays are simple to run and require little specialized expertise.

2.2.1.2.1. Preparation of reagents and sample analysis. The malachite green solutions were prepared by diluting 43.75 mL 96% H_2SO_4 with ultrapure water to 200 mL total volume. For the PVA assay, then 27 g ammonium molybdate tetrahydrate and 0.135 g malachite green oxalate salt were added to the diluted acid. In the SDS-supplemented assay, 20.25 g ammonium molybdate tetrahydrate and 0.10125 g malachite green oxalate salt were used instead. The resulting solution was diluted to 500 mL with ultrapure water and mixed. The solution was stored at 4 °C overnight, and then filtered through a 0.2 μm a PES filter. A 0.1% solution of PVA was made in 80 °C ultrapure water to ensure dissolution, and allowed to cool down. The 0.02% SDS solution was prepared and stored at room temperature. Additional stock solutions were "low acidity" H_2SO_4 (1.8 M for both PVA and SDS assays), "high acidity" H_2SO_4 (4.5 M for PVA and 3.6 M for SDS), and a 0.75% oxalic acid solution. On the day of measurement, reagents were prepared as follows: 1.0 mL Malachite Green solution, 1.0 mL surfactant (PVA or SDS) solution, 0.75 mL acetone, 0.75 mL oxalic acid (0.75%), 1.5 mL ultrapure water. High and low acidity reagents were prepared separately by either adding 1 mL of the highly concentrated or 1.8 M H_2SO_4 solution, respectively.

In a clear, flat-bottom 96-well microtiter plate, 50 μL of sample and 100 μL of low acidity reagent were pipetted. In a separate well, 50 μL of the same sample and 100 μL of high acidity reagent were added. The plate was kept in the dark for 3 h and subsequently absorbance was measured using an InfiniteM200Pro microplate reader (TECAN, Switzerland). Absorbance was measured according to Fig. 2 (e.g. at 560 nm and 620 nm for samples treated with low acidity reagent in the PVA supplemented assay).

Afterwards, 12.5 μL 7.8 mM KIO_3 was added to wells with low acidity reagent, and kept in the dark for 3.5 h. Then, absorbance spectra of the oxidized low acidity reagent were measured according to Fig. 2.

Standards of As(V), As(III) and PO_4^{3-} were prepared in the same salinity and sulfate concentration as the samples measured, in a range of 1–40 μM for the PVA-supplemented reagents and 0.1–15 μM in the SDS-supplemented reagents. In the PVA-based assay As(V) and PO_4^{3-} standards were measured in all reagents. Arsenite standards were only measured in the low acidity reagent after oxidation, since it never showed absorbance in any reagent before the oxidation step, which implies that ε_L was always zero. In the SDS-based assay, PO_4^{3-} standards were measured in all reagents, As(V) and As(III) standards were measured in low acidity reagent before and after oxidation (according to Eqs. (13)–(15)), since α_H in Eq. (13) was always zero but ε_L in Eq. (15) was not. Standards were measured simultaneously with samples, using the same reagents.

2.2.1.2.2. Calculation for PVA-supplemented assay. Regression coefficients (slopes and intercepts) of each analyte in each reagent mixture were obtained using the standards and by fitting the AI data according to the Eqs. (3)–(10) (see also Supp. Table S1). Since As(III) never showed an absorbance signal in the low acidity reagent, ε_L is zero and regression according to Eq. (7) can be omitted. Eqs. (13)–(15) are thus simplified to

$$AI_H = \alpha_H \times [As(V)] + \gamma_H \times \left[PO_4^{3-}\right] + \Phi_H \quad (16)$$

$$AI_L = \alpha_L \times [As(V)] + \gamma_L \times \left[PO_4^{3-}\right] + \Phi_L \text{ and} \quad (17)$$

$$AI_{LO} = \alpha_{LO} \times [As(V)] + \varepsilon_{LO} \times [As(III)] + \gamma_{LO} \times \left[PO_4^{3-}\right] + \Phi_{LO}. \quad (18)$$

Concentrations of the analytes in samples with unknown composition were then determined by measuring the absorbance index in all three reagent mixtures, and substituting in the coefficient values. Eqs. (16)–(18) are then solved for $[PO_4^{3-}]$, [As(V)] and [As(III)], which gives

$$\left[PO_4^{3-}\right] = \frac{\alpha_H \times (AI_L - \Phi_L) - \alpha_L \times (AI_H - \Phi_H)}{\gamma_L \times \alpha_H - \alpha_L \times \gamma_H} \quad (19)$$

$$[As(V)] = \frac{-\left[PO_4^{3-}\right] \times \gamma_L + AI_L - \delta_L}{\alpha_L} \quad (20)$$

$$[As(III)] = \frac{-[As(V)] \times \alpha_{LO} - \left[PO_4^{3-}\right] \times \gamma_{LO} + AI_{LO} - \Phi_{LO}}{\varepsilon_{LO}} \quad (21)$$

By then replacing AI_H, AI_L, AI_{LO}, and the regression coefficients with the known values, all analyte concentrations in the samples can be found.

Regression Eqs. (3)–(10) work best at analyte concentrations <7.5 μM. For higher concentrations, it is recommended to use modified regression equations. Namely, taking the natural log of both concentration and AI values for standards of each analyte is recommended before fitting the data to a linear regression model (Supp. Table S1). For instance, if PO_4^{3-} > 7.5 μM, the calibration equation for PO_4^{3-} in the oxidized low acidity reagent (Eq. (8)) would change to

$$\log\left(AI_{LO}\left(PO_4^{3-}\right)\right) = \gamma_{LO} \times \log\left(\left[PO_4^{3-}\right]\right) + \delta_{LO} \quad (22)$$

which can also be shown as

$$AI_{LO}\left(PO_4^{3-}\right) = e^{\gamma_{LO} \times \log\left(\left[PO_4^{3-}\right]\right) + \delta_{LO}}, \quad (23)$$

This implies that δ_{LO} cannot easily be integrated into Φ_{LO} in Eq. (18). Empirically, results were best when Φ_{LO} is the average of only the non-log y-intercepts of As(V) and As(III) and when subtracting the AI of the blank in the oxidant-supplemented reagent (AI_{LO_blank}), which gives

$$AI_{LO} = \alpha_{LO}[As(V)] + \varepsilon_{LO}[As(III)] + \Phi_{LO} + e^{\gamma_{LO} \times \log\left[PO_4^{3-}\right] + \delta_{LO}} - AI_{LO\_blank}, \quad (24)$$

Regressions using the natural log cannot be used for AI in the high and low acidity reagents (Eqs. (16)–(17)) because the set of equation does not have a closed-form solution. Given that Eqs. (19)–(20) are solved as shown above, Eq. (21) changes to

$$[As(III)] = e^{\frac{AI_{Blank,LO} - [As(V)] \times \alpha_{LO} + AI_{LO} - \Phi_{LO} - e^{\delta_{LO} + \gamma_{LO} \times \log\left(\left[PO_4^{3-}\right]\right)}}{\varepsilon_{LO}}} \quad (25)$$

Equations solved for [As(V)], [As(III)] and $[PO_4^{3-}]$ for all possible concentration ranges may be found in Supp. Table S1.

The concentration-dependent choice of AI and type of regressions implies that the analysis workflow was dynamic, and calculations were refined stepwise for each sample (Fig. 2). First, AI_H, AI_L and AI_{LO} were calculated according to the first arrow in Fig. 2 using the set of Eqs. (13)–(15). If PO_4^{3-} < 0.1 μM, AI_H, AI_L and AI_{LO} were recalculated using different absorbance wavelengths. Finally, if concentrations of [As(V)], [As(III)] or $[PO_4^{3-}]$ were > 7.5 μM, regressions based on the natural log were chosen, if solving the set equations was still possible (for example, Eq. (25)). This analysis path can be found by consulting Fig. 2 and Supp. Table S1, and we also provide an excel template that automates the analysis as Supplement 2.

2.2.1.2.3. Calculation for SDS-supplemented assay. Regression coefficients (slopes and intercepts) of each analyte in each reagent mixture were obtained using the standards and by fitting the AI data according to the Eqs. (3)–(10) (see also Supp. Table S1). Since As(V) never showed an absorbance signal in the low acidity reagent, α_H is zero and regression according to Eq. (4) can be omitted. Eqs. (13)–(15) are thus simplified to

$$AI_H = \gamma_H\left[PO_4^{3-}\right] + \delta_H \quad (26)$$

$$AI_L = \alpha_L[As(V)] + \varepsilon_L[As(III)] + \gamma_L\left[PO_4^{3-}\right] + \Phi_L \quad (27)$$

$$AI_{LO} = \alpha_{LO}[As(V)] + \varepsilon_{LO}[As(III)] + \gamma_{LO}\left[PO_4^{3-}\right] + \Phi_{LO} \quad (28)$$

Concentrations of the analytes in samples with unknown composition were then determined by measuring the absorbance index in all three reagent mixtures, and substituting in the coefficient values. Eqs. (26)–(28) were then solved for $[PO_4^{3-}]$, [As(V)] and [As(III)]:

$$\left[PO_4^{3-}\right] = \frac{AI_H - \delta_H}{\gamma_H} \quad (29)$$

$$[As(V)] = \frac{-\varepsilon_L \times \left(\left[PO_4^{3-}\right] \times \gamma_{LO} - AI_{LO} + \phi_{LO}\right) + \varepsilon_{LO} \times \left(\left[PO_4^{3-}\right] \times \gamma_L - AI_L + \phi_L\right)}{\varepsilon_L \times \alpha_{LO} - \alpha_L \times \varepsilon_{LO}} \quad (30)$$

$$[As(III)] = \frac{[As(V)] \times \alpha_{LO} - \left[PO_4^{3-}\right] \times \gamma_{LO} + AI_{LO} - \Phi_{LO})}{\varepsilon_L} \quad (31)$$

Similar to the calculations for the PVA assay (2.2.1.2.1), Eqs. (29)–(31) work best at analyte concentrations below a certain threshold, which was 1 μM for the SDS-supplemented assay. For higher concentrations (>1 μM), it is recommended to use modified regression equations. Concentrations of As(V), PO_4^{3-} and As(III) were thus calculated from Eqs. (29)–(31), but modified according to Supp. Table S1 when use of the natural log was possible. Based on the initial results, the calculation of AI_L and AI_{LO} were refined for each sample (Fig. 2). An excel spreadsheet automating this refinement is available as Supplementary material 2.

2.2.2. Application in contaminated soils

2.2.2.1. Site description. Samples were taken in March 2021 from the Bossegraben (51.899°N, 10.498°E) (Fig. 3, Supp. Fig. S14), a small brook near Oker, in Germany, which originates in the Harz mountains and merges with the river Röseckenbach. Based on personal communication (2021) with the Fachbereich Bauen & Umwelt - Bodenschutz / Deponiemanagement and Fachbereich Umwelt und Gewässerschutz, Landkreis Goslar, the historical context of the site was gathered. The Bossegraben passes along a depot where mining waste disposal took place in the 1950s to 70s. Upon the discovery of As contamination in the Bossegraben and Röseckenbach, the southern part of this mining depot was been sealed with clay in an attempt to decrease the input of As into the adjacent waters. The remaining low concentrations of As that are still detected possibly originate from remaining particulates in the river beds or are supplied by rainfall that percolates through the northern side of the mining depot and carries dissolved metals and As into the Bossegraben. Additionally, As has been reported in the groundwater of the Harz Mountain region, and its surfacing may also contribute to the elevated levels of As in the brook. Further actions to minimize As contamination of the Bossegraben, Röseckenbach, and groundwater will be executed by fall 2022.

2.2.2.2. Sampling. Soil cores (2.5 cm diameter, depth 3 to 5 cm) were taken in quadruplicate at five sites along the brook (Fig. 3, Supp. Fig. S14), with site 1 being a reference site without anticipated As contamination. Cores

Fig. 3. Maps of sampling sites 1–5 in the Bossegraben brook near Oker, Germany, with the potentially arsenic-contaminated Schrevenwiesen deposit site marked in yellow, and the larger Röseckenbach river into which the Bossegraben flows (upper panel). A spring of water located upstream of site 2 is also noted in yellow. Sampling sites and example sediment cores pictured on the day of sampling are shown in Fig. S14.

were transported upright and cooled by icepacks to the laboratory facilities in Bremen. On the same day, microsensor depth profiling was performed on one of the cores per site and porewater was extracted at every 0.5 cm from three cores per site using rhizones (Rhizosphere Research Products, Netherlands). From each porewater sample, 100 μL were fixed with 1% zinc acetate for sulfate measurements, 100 μL were immediately used for Fe analysis and the remaining ~800 μL were immediately transferred into cryovials, flash frozen in liquid nitrogen and kept at −80 °C until determination of As concentration. 200 μL were used for determination with the colorimetric assay described here. The remaining volume was used for total As and for As speciation determination using ICP-MS at Universität Bayreuth. While that large sample volume had the disadvantage of a loss of depth resolution ('smearing'), the ICP-MS analyses allowed to validate the results of the colorimetric assay on the same core.

2.2.2.3. Porewater analysis. Dissolved Fe in porewater samples was analyzed according to Viollier et al. (2000). The reductant hydroxylamine was added to the colorimetric reagent mixture, under the assumption that any dissolved Fe in the sample is Fe(II) due to exposure of the sample to air during sampling (Albrechtsen and Christensen, 1994). Porewater samples fixed in zinc acetate were diluted to 10 mL with ultrapure water for sulfate measurement by ion chromatography (Metrohm 930 Compact IC Flex). After thawing, 100 μL per sample were analyzed in duplicate using the novel colorimetric SDS assay following the analytical flowchart (Fig. 2) developed in this study.

IC measurements showed an average sulfate concentration of 775 μM. Hence, standards of 0.5–7.5 μM As(III), As(V) and PO_4^{3-} were made in 775 μM sulfate solution, and run in parallel with the samples during the colorimetric analyses. Each sample subset was analyzed in low and high acidity reagents. After 3 h of reaction time, absorbance was measured according to Fig. 2. Then, 12.5 μL 7.8 mM KIO_3 were added to samples and standards treated with low acidity reagent immediately after measurement. Plates were kept in the dark for 3 h, after which absorbance was measured again. The diagram on Fig. 2 was followed for regression modelling.

2.2.2.4. Validation with ICP-MS. Arsenic speciation was determined by high performance liquid chromatography (HPLC; 1260 Infinity II bio inert, Agilent) using a PRP-X100 column (Hamilton 5 μm, 10 mM NH_4NO_3, 10 mM $NH_4H_2PO_4$, and 500 mg/L Na_2-EDTA at a flow rate of 1.0 mL/min and 25 μL injection volume) (Van de Wiele et al., 2010) coupled to ICP-MS/MS (8900 Triple Quadrupole, Agilent). Arsenic was detected in MS/MS mode using oxygen as reaction cell gas (AsO^+, *m/z* 75 - > 91). Retention times of arsenite and arsenate were determined using individual standards. Samples stabilized in 2% HNO_3 were analyzed for total As concentrations by ICP-MS/MS using Rhodium (Rh) as an internal standard (AsO^+, m/z 75 - > 91; Rh^+ 103 - > 103).

2.2.2.5. Microsensor measurements. Oxygen, H_2S and pH microsensors with a tip diameter of 50–100 μm were constructed, calibrated and used as described previously (De Beer et al., 1997; Jeroschewski et al., 1996; Klatt et al., 2016; Revsbech, 1989). Depth profiles were measured in triplicate at two spots per core. All sensors were mounted on a multi-sensor holder and the distance between the tips was ~1 cm. The calculation of total sulfide (ΣH_2S, HS^-, S^{2-}) from pH and H_2S depth profiles was not attempted due to the lateral heterogeneity of the soil samples.

3. Results and discussion

3.1. Limits of the novel colorimetric method

Measured concentration and limit of detection (LoD) were strongly dependent on the wavelengths measured, and varied with analyte type and reagent mixture due to differences in spectral shape. Therefore calculations based on carefully optimized specific wavelengths (Fig. 2) are recommended, instead of only measuring the maximum absorbance at a single wavelength as is commonly done in colorimetric methods. A flowchart was devised to help navigate the choice towards the most accurate combination of calculations (Fig. 2). An example of the usage of this flowchart can be found in the Supp. to Materials and Methods (1.3). Despite optimization across a series of conditions, we encourage the user to reevaluate absorbance choice and to test the method in certified reference material analogous to the sample, if samples are in a particularly complex matrices that affect spectral shape (see Supp. Fig. S1).

In samples containing only one analyte, LoD of As(V) was 0.11 μM and LoD of As(III) was 0.44 μM using the PVA-supplemented assay, while LoD of As(V) was 0.07 μM and LoD of As(III) was 0.06 μM in the SDS-supplemented assay (see Supp. Materials and Methods (1.9 for calculation). LoD could be lowered by using 1.5 mL cuvettes: In the PVA assay, the LoD of As(V) was 0.1 μM; and in the SDS assay the LoD of As(V) was 0.04 μM (protocol in Supp. Materials and Methods 1.4) using the wavelengths indicated in Fig. 2.

The dependency of each absorbance index on analyte concentration changes with analyte and reagent mix. Consequently, accuracy of measurements differed based on background values of PO_4^{3-}, high As(V) or high As(III) (Fig. 4, Supp. Figs. S11 & S12, Supp. Table S2). The presence of multiple analytes had a negative effect on LoD compared to pure standards, particularly in the PVA-supplemented assay (Supp. Table S2). Yet, measurements of As(V) and As(III) were accurate when choosing spectral indices based on the type and concentration of the analytes and corresponding reagent mixtures. In mixtures of As(V) and As(III) with up to 5 μM PO_4^{3-}, LoD for As(V) in the PVA-supplemented assay

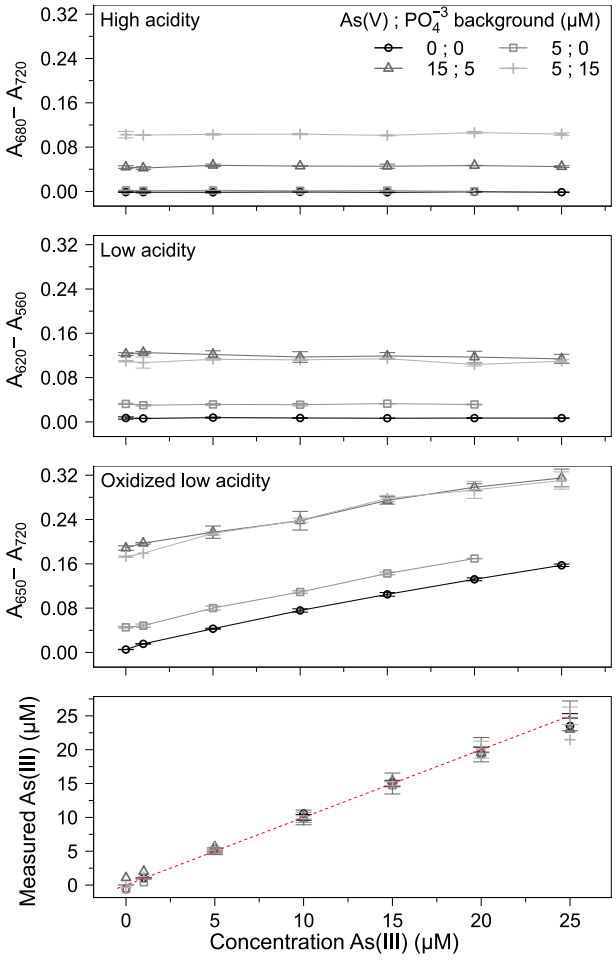

Fig. 4. Effect of background As(V) and PO_4^{3-} interference on As(III) measured using the PVA-supplemented assay in high acidity (top panel), low acidity (second panel), low acidity after oxidation (third panel), as well as the final calibration curve (bottom panel) in which the dotted red line represents a 1:1 agreement between measured and actual As(III) concentration, $n = 3$. The absorbance indices used for each reagent are noted on the y-axis, e.g. difference in absorbance at 680 nm and absorbance at 750 nm in the high acidity reagent.

increased to 0.47 μM, and for As(III) to 0.56 μM. In the presence of 15 μM PO_4^{3-}, LoD increased further by a factor of up 5 (Supp. Table S2). Increasing concentrations of the other arsenic species had less fundamental effect on LoD of As(V) and As(III) (Supp. Table S2). In the SDS-supplemented mixtures, the pattern was similar. Yet, LoD of all analytes always stayed below 1 μM (Supp. Table S2). In all combinations, R^2 was higher than 0.9. The standard error of the estimate was less affected than LoD because concentrations above the LoD could accurately be predicted (Supp. Table S2).

Interference from Si, Fe and H_2S was negligible after optimization of the reagent mixture composition (Supp. Table S3, details of testing protocol in Supp. Materials and Methods 1.7). At the indices suggested for analysis (Fig. 2), sulfate interference played a minimal role in As(V) recovery, in both 1× and 2× ASW salinities (Supp. Fig. S7). Thus, PO_4^{3-} and As(V) concentration in samples of unknown composition can be determined using calibration regressions of standards in ultrapure water, at the cost of an increase in LoD for the SDS-supplemented assay. Arsenite recovery in saltwater was highly inaccurate in both methods (Supp. Fig. S7) when calculated using standards in ultrapure water, because the efficiency of As(III) oxidation was strongly dependent on salinity. Further research on alternative oxidants is necessary to address this issue. This limitation does not impede analysis of samples for the PVA-supplemented assay, given that salinity and sulfate concentration are known. Measurement of As(III) with the SDS-supplemented assay is not recommended for samples with salinity ≥35 g/L.

Adaptation of this method for use with larger volumes of water and preconcentration, or selective filtration, may increase sensitivity if determination of potable water is desired. Currently, sample matrix composition is a dictating factor in the LoD of this method, and plays an important role in determining whether this method is suitable for detection of As in potable water according to WHO guidelines. In PO_4^{3-}-free samples, LODs below WHO guidelines were achieved, and they were close to guidelines in samples with concentrations of PO_4^{3-} below 1 μM. Further optimization of reagent mixture composition will likely allow to use this assay for drinking water quality testing, given that salinity and sulfate levels of the samples are known.

3.2. Validation of colorimetric assay in natural porewater samples

Results of the colorimetric assay for a subset of Bossegraben soil porewater were compared to the results of total As determination and As speciation by ICP-MS. Recovery of total As by colorimetry, calculated as the sum of As(III) and As(V) concentration, was in agreement with totals derived from ICP-MS for As over 0.5 μM (Supp. Table S4). Below 0.5 μM, both As(V) and As(III) may be overestimated due to the complex matrix and PO_4^{3-} background, resulting in inaccurate values of total arsenic.

The speciation analysis results by ICP-MS were also in agreement with those measured with the colorimetric method (Supp. Table S4). For As(V), these measurements differed by only 11 ± 26% on average, including the concentrations close to the detection limit. For As(III), speciation measurements differed by 41 ± 30%. Yet, this number reflects differences of only 0.32 ± 0.43 μM. The percentages were high because As(III) was close to detection limit in most samples. Arsenate and As(III) measured by colorimetry and ICP-MS therefore picked up the same trends with site and depth (Fig. 5). Measured As appeared to be mostly independent of PO_4^{3-}, although some interference is expected when PO_4^{3-} is above 7.5 μM, like in Site 2. Due to interference, it is expected that As(V) values would be overestimated, while As(III) would be underestimated. In Site 5, which had a PO_4^{3-} background of only up to 2 μM, the average difference between As(V) measured by ICP-MS compared to the novel method was 0.18 ± 0.14 μM. The average difference for As(III) was 0.12 ± 0.08 μM. Speciation results by ICP-MS and colorimetry were thus in closest agreement despite the low As concentrations, which emphasizes the strength of the novel method in the presence low PO_4^{3-}, even if it still overwhelms the concentration of the As species.

3.3. As mobility in the Bossegraben

In all cores, O_2 was rapidly depleted within the uppermost 1 cm, which was accompanied by a gradual decrease of pH with depth (Fig. 6). Porewater As, PO_4^{3-} and Fe depth profiles of all sites were highly heterogenous (Fig. 5), despite the close proximity in which replicate soil cores where taken. This heterogeneity could be due to the roots of plants or hotspots of organic material degradation. Also, the hydrological settings in terms of advective groundwater upflow after precipitation and runoff events, spring distribution and lateral spreading of brook water, plausibly affect local solute distribution. The water column and depth distribution of As between sites were clearly distinct (Fig. 5 & 7). In the anticipated reference site, (site 1, Fig. 5), As concentrations in the water column were close to the detection limit (<0.1–0.4 μM), showing values close to the natural background (Harzwasserwerke GmbH, 2021). Especially site 2 showed As concentration of 4.6 ± 1.9 μM in the water column, far outreaching the natural background concentration. Even though the As concentration in the water column decreased further downstream, values were still elevated compared to background levels and drinking water standards.

Arsenic concentration in the porewater of reference site also showed abundance in the range of natural background in reducing soil (0.19 ±

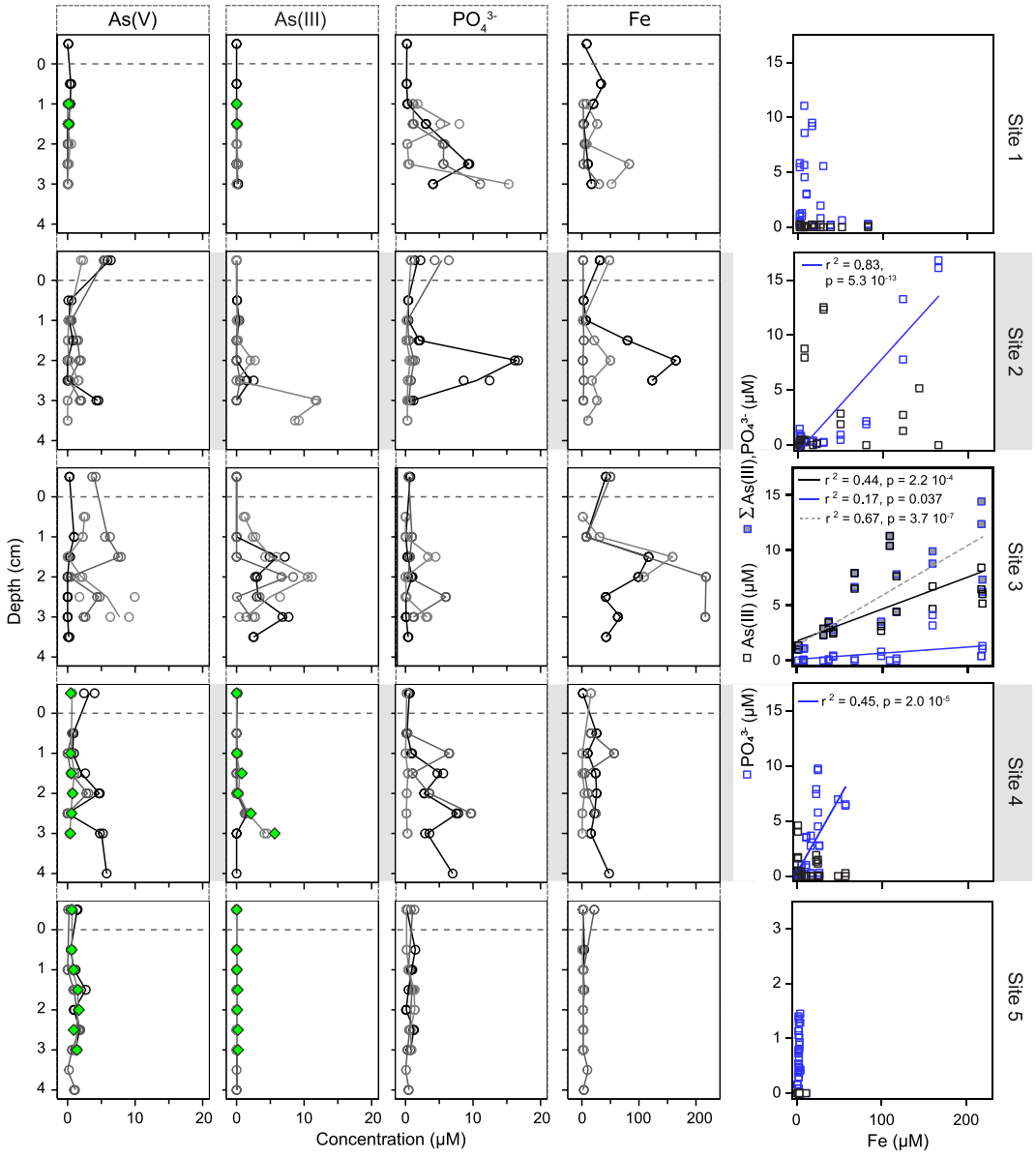

Fig. 5. Concentration of As(V), As(III), PO_4^{3-}, total dissolved Fe over depth, in the five sites along the Bossegraben brook. Concentration was measured in porewater extracted from three sediment cores per site, with each line and shade of the symbols in each panel representing one core. Each sample was measured in duplicate per core for arsenic speciation and phosphate with the colorimetric SDS-supplemented assay, while single measurements per core were done for Fe. Arsenic speciation with ICP-MS (green markers) was only done on one core per site (see Supp. Table S4). Analysis (right panels) of the dependency of As(III) and PO_4^{3-} concentration on dissolved Fe was done using all three cores per site. For site 3, the sum of As(III) and PO_4^{3-} is included because of an increased significance of the correlation compared to only phosphate or only As(III), which indicates release of both compounds during reductive dissolution of oxidized Fe. The linear regression model was only included in the graphs for *p*-values lower than 0.05. See Fig. S13 for correlation analysis of As(V).

0.18 μM). In site 2, porewater As concentrations were slightly elevated (0.55 ± 0.4 μM) in the uppermost 2 cm, but then increased sharply to up to ~12 μM. Despite the decreased water column arsenic concentration in site 3, porewater arsenic concentrations were highest throughout the soil (average 6.1 ± 3.4 μM). Even in layers close to the water column interface at 0.5 cm depth concentration reached up to 4.1 μM, exceeding the water column values (2.1 ± 1.6 μM) (Fig. 7). Sites downstream of site 3 showed a gradual decrease in porewater As concentration.

While As(V) was the dominant As species in the oxic water column, As(III) was dominant in the porewater in sites 2 and 3 (Fig. 5), consistent with the reducing environment. At site 4, however, As(V) and As(III) were both abundant. In site 5, the soil porewater was depleted in total arsenic compared to the water column (Fig. 7B), and As(V) dominated over As(III).

3.3.1. Sources and sinks of arsenic in the Bossegraben

In site 2, porewater Fe was highly correlated to PO_4^{3-} but not to any of the As species, (Fig. 5, Fig. S13). This suggests that sorbed PO_4^{3-} is released by reductive dissolution of oxidized Fe, while As has a different source. Given that As in water column exceeded the porewater concentration, an inflow of As from the contamination source, maybe by surface water, is likely. This is further supported by a drastic change of water column pH from ~7.7 to 8.2 at site 2 that then deceased again along the brook's flow path, and by the observation of a nearby spring that emerges close to the slope of the sealant clay hill (Supp. Fig. S15) and merges with the Bossegraben right before site 2.

The brook has a long history of exposure to arsenic, opening two plausible scenarios of As sources at site 3. First, the As-containing iron minerals might originate directly from the waste deposit, and were carried into the

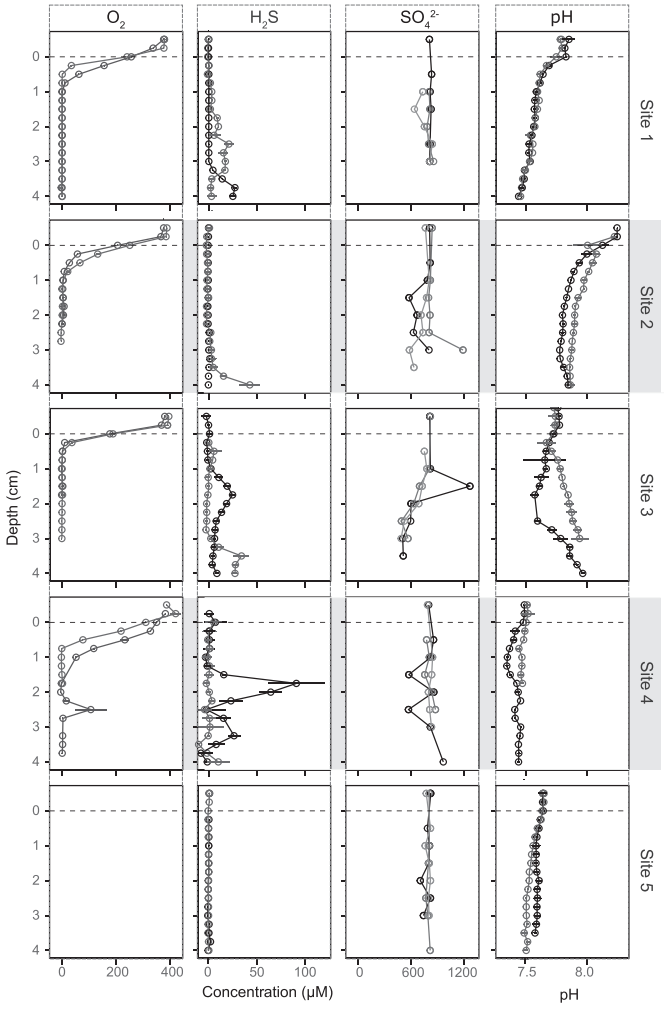

Fig. 6. Concentration of O_2, H_2S, SO_4^{2-} and pH through depth, in five sites along the Bossegraben brook in the Harz mountains, Germany. SO_4^{2-} concentration was measured in porewater extracted from three sediment cores per site, with each line in the graph representing one core (n = 3). O_2, H_2S and pH were measured with microsensors in one core per site, each line represents one location within the core (n = 2, with 3 measurements per location; error bars represent standard deviation). The dashed horizontal lines indicate the soil surface, with negative depth values referring to the water column and positive values referring to the depth of porewater sampling relative to the sediment surface at depth 0 cm.

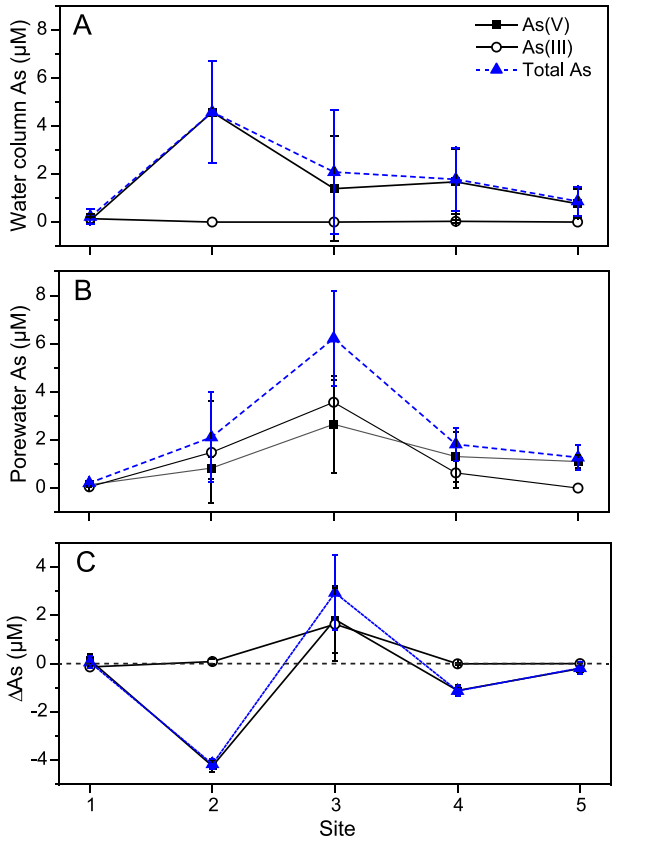

Fig. 7. Change in concentration and concentration gradients of As(III) and As(V), and their sum (total As), along the flow bath of the brook. In A) water column concentration is shown, while B) shows the average concentration of the arsenic species in porewater throughout the core. In C) the concentration gradient across the soil surface (ΔAs) was calculated by subtracting the water column concentration from the porewater concentration at the depth closest to the surface. A negative ΔAs value therefore approximates that there is a net uptake flux of the soil, while positive values indicate release. In all panels, the error bars represent standard deviation (n = 3, based on three cores, excluding the error based on replicate porewater samples and multiple depths).

brook bed by fluvial transport and runoff before the clay sealing was built. The alternative scenario considers that As concentrations in the brook water were substantially higher before the remediation measures were taken (Fachbereich Bauen & Umwelt - Bodenschutz / Deponiemanagement and Fachbereich Umwelt und Gewässerschutz, Landkreis Goslar, personal communication, 2021). Percolating dissolved arsenic would have sorbed to the naturally abundant and clay-derived Fe minerals, either in the form As(V) or As(III) that both have similar sorption behavior at the measured soil pH (Dixit and Hering, 2003).

Porewater As(III) and PO_4^{3-} were correlated to dissolved Fe concentration (Fig. 5). Particularly the sum of both was linearly dependent on Fe, suggesting that both As and PO_4^{3-} are released during reductive dissolution of As containing Fe-minerals. The co-occurrence of As(V) despite the reducing conditions suggests a local release by reductive dissolution (Lopez-Adams et al., 2021; Nicholas et al., 2003). Arsenate tends to remain oxidized when sorbed, and upon reductive dissolution of the Fe minerals it becomes available for reduction, e.g., by microbial respiration (Lopez-Adams et al., 2021; Mazumder et al., 2020). A mixture of As species is thus expected close to the site of dissolution, even under highly reducing conditions as is the case here. Upwelling groundwater percolating through mineral-sorbed As layers elsewhere may carry both solutes into the measured porewater space.

Independent of the type of processes releasing arsenic at depth, the concentration gradient across the soil interface (Fig. 7B) suggests net release by the soil. Higher depth resolution and a characterization of the dominant mass transfer phenomena would, however, be needed to quantify interfacial fluxes. Net export of Fe is further supported by the observation of orange flocs on the soil surface of site 3 that indicate accumulation of oxidized iron upon surfacing of the dissolved reduced species, which is expected to resorb a substantial fraction of the released arsenic and prevention of downstream transport.

Site 4 was still influenced by the contamination. O_2 penetrated deeper than at the other sites, but the dependence of PO_4^{3-} concentration on dissolved Fe suggests a reducing environment at depth. Yet, abundance of the arsenic species was not significantly correlated to Fe, suggesting negligible ongoing release during reductive dissolution. Also, As(V) concentrations exceeded the concentrations of As(III), which might point towards upwelling of less reduced arsenic-rich groundwater. However, the dissolved As did not reach the soil surface, and concentrations of As in the porewater in the uppermost layers were lower than in the water column. This indicates net uptake of water column As by the soil. Thus, the As released upstream may be resorbed or complexed. Because sulfide only occurs in distinct patches that are plausibly related to the decay of organic matter deposits (desulfurization), it is unlikely to play an important in scavenging As by

formation of AsS minerals. Instead, the dominant sink is likely resorption to iron minerals and natural organic matter (NOM) (Eberle et al., 2021).

At site 5 barely any free PO_4^{3-} and Fe were detectable in the porewater, suggesting less reducing conditions, which would further favor the resorption of As delivered from the water column upstream. In addition to resorption, dissolved water column As is likely diluted as Bossegraben water mixes with surrounding low-As groundwater in sites 4 and 5. A substantial contribution to the decrease in As is, however, unlikely because brook width and water flow substantially decrease towards site 5 (see photos in Fig. S4). While the exact mechanism behind As retention remains to be illuminated, our data overall show that the Bossegraben soil changes from a source to sink along the flow path (Fig. 7). It remains to be clarified whether the As contamination is still spreading and might not have reached site 4 and 5 yet.

4. Conclusions

The detection of As in samples of 100 μL volume was achieved using two different surfactants, suitable for distinct concentration ranges: ~1–40 μM (PVA) and ~ 0.1–15 μM (SDS). Through a targeted selection of spectral features, interference from silicate, sulfate, iron, and sulfide, as well as from a PO_4^{3-} background was minimized (Fig. 2). The PVA-based approach appears to be the most robust of the two, especially because salinity has a very limited effect on the limits of detection using this assay. Additionally, the effect of analyte type and concentration on spectral shape is limited, which minimizes the number index combinations required. Yet, the SDS-based approach achieves substantially lower detection limits.

The greatest advantage of this method over previous colorimetric methods (Supp. Table S5) for the detection of As is the extremely low sample volume needed. This method requires only 100 μL of sample, which makes it ideal for assessing arsenic levels in soils and sediments using porewater. Through the use of a novel colorimetric method, the sources and sinks of arsenic in Bossegraben Brook could be tracked both at a cm-scale through depth, and at a meter scale across five sampling sites. Comparison of fine-scale arsenic dynamics to changes in iron, sulfide, sulfate, pH, and oxygen were possible without access to expensive and specialized equipment, and was cost- and time-efficient. The analysis showed that arsenic input occurs directly into the water column, likely from a spring (Site 2), and from the soil (Site 3). Release of As(V) from the soil is likely the result of reductive Fe-mineral dissolution. Released As(V) is plausibly microbially oxidized to As(III) in the porewater. Upwelling groundwater rich in As could contribute to additional As input in site 3 and 4. Arsenic concentration decreased before reaching the Röseckenbach, likely due to sorption with iron and additional dilution with low-As groundwater. This study highlights that spatially resolved descriptions of the cycling of As in sediment and soil can help understand the mechanisms behind As export and uptake. The novel colorimetric assay can thus facilitate studies that aim to describe mechanisms of As release, and potentially be used to assess the risk of enhanced As mobility when favorable conditions are present in an area of interest.

CRediT authorship contribution statement

Andrea Castillejos Sepúlveda: Data curation, Validation, Investigation, Visualization, Writing – original draft, Writing – review & editing. **Lais M. Gatti:** Methodology, Validation, Investigation. **Carolin F. Kerl:** Formal analysis, Validation, Writing – review & editing, Resources. **Arjun Chennu:** Software, Formal analysis, Writing – review & editing. **Judith M. Klatt:** Supervision, Conceptualization, Methodology, Investigation, Formal analysis, Validation, Investigation, Visualization, Writing – original draft, Writing – review & editing, Funding acquisition.

Declaration of competing interest

The authors declare that they have no known competing financial interests or personal relationships that could have appeared to influence the work reported in this paper.

Acknowledgements

The authors would like to thank the Landkreis Goslar, Fachbereich Bauen & Umwelt - Bodenschutz / Deponiemanagement and Fachbereich Umwelt und Gewässerschutz, particularly W. Schmotz, D. Sielaff, M. Delius and M. Kunze, as well as F. Knolle for guidance and support in field sampling, G. Eickert-Grötzschel, K. Hohmann, V. Hübner, A. Niclas, I. Schröder, C. Wigand for microsensor construction, M. Alisch for sulfate measurements, and D. Schürholz for help with software development. The authors also thank D. de Beer and B. Planer-Friedrich for their analytical insight and constructive input, and B. Kartal for access to laboratory facilities. This research was supported by the Max Planck Society.

Appendix A. Supplementary data

Supplementary data to this article can be found online at https://doi.org/10.1016/j.scitotenv.2022.154155.

References

Albrechtsen, H.J., Christensen, T.H., 1994. Evidence for microbial iron reduction in a landfill leachate-polluted aquifer (Vejen, Denmark). Appl. Environ. Microbiol. 60.

Altmann, H.J., Fürstenau, E., Gielewski, A., Scholz, L., 1971. Photometrische Bestimmung kleiner Phosphatmengen mit Malachitgrün. Fresenius' Z. Anal. Chem. 256, 274–276. https://doi.org/10.1007/BF00537892.

Barnes, J.W., Murray, C.W., 1930. Accuracy of the gutzeit method for the determination of minute quantities of arsenic. Ind. Eng. Chem. Anal. Ed. 2, 29–30. https://doi.org/10.1021/ac50069a012.

Bednar, A.J., Garbarino, J.R., Ranville, J.F., Wildeman, T.R., 2002. Preserving the distribution of inorganic arsenic species in groundwater and acid mine drainage samples. Environ. Sci. Technol. 36, 2213–2218. https://doi.org/10.1021/es0157651.

Blomqvist, S., Hjellström, K., Sjösten, A., 1993. Interference from arsenate, fluoride and silicate when determining phosphate in water by the phosphoantimonylmolybdenum blue method. Int. J. Environ. Anal. Chem. 54, 31–43. https://doi.org/10.1080/03067319308044425.

Bundschuh, J., Litter, M.I., Parvez, F., Román-Ross, G., Nicolli, H.B., Jean, J.S., Liu, C.W., López, D., Armienta, M.A., Guilherme, L.R.G., Cuevas, A.G., Cornejo, L., Cumbal, L., Toujaguez, R., 2012. One century of arsenic exposure in Latin America: a review of history and occurrence from 14 countries. Sci. Total Environ. https://doi.org/10.1016/j.scitotenv.2011.06.024.

Carter, S.G., Karl, D.W., 1982. Inorganic phosphate assay with malachite green: an improvement and evaluation. J. Biochem. Biophys. Methods 7, 7–13. https://doi.org/10.1016/0165-022X(82)90031-8.

De Beer, D., Schramm, A., Santegoeds, C.M., Kuhl, M., 1997. A nitrite microsensor for profiling environmental biofilms. Appl. Environ. Microbiol. 63.

Deicke, M., Ruppert, H., 2013. Bergbau- und Umweltgeschichte des Oberharzes (Exkursion L am 6. April 2013). Jahresberichte und Mitteilungen des Oberrheinischen geol. Vereins 95, 259–288. https://doi.org/10.1127/JMOGV/95/2013/259.

Dixit, S., Hering, J.G., 2003. Comparison of arsenic(V) and arsenic(III) sorption onto iron oxide minerals: implications for arsenic mobility. Environ. Sci. Technol. 37, 4182–4189. https://doi.org/10.1021/es030309t.

Eberle, A., Besold, J., León Ninin, J.M., Kerl, C.F., Kujala, K., Planer-Friedrich, B., 2021. Potential of high pH and reduced sulfur for arsenic mobilization – insights from a finnish peatland treating mining waste water. Sci. Total Environ. 758, 143689. https://doi.org/10.1016/J.SCITOTENV.2020.143689.

Goldstone, N.I., 1946. A source of error in the gutzeit method for arsenic. Ind. Eng. Chem. Anal. Ed. 18, 797–799. https://doi.org/10.1021/i560160a020.

Gómez, M., Cámara, C., Palacios, M.A., López-Gonzálvez, A., 1997. Anionic cartridge preconcentrators for inorganic arsenic, monomethylarsonate and dimethylarsinate determination by on-line HPLC-HG-AAS. Fresenius J. Anal. Chem. 357, 844–849. https://doi.org/10.1007/s002160050260.

Harzwasserwerke GmbH, 2021. Harzwasserwerke GmbH - Trinkwasseranalysen [WWW Document]. https://www.harzwasserwerke.de/unser-wasser/herrlich-weiches-wasser/trinkwasseranalysen/ (accessed 2.8.22).

Hossain, M., Williams, P.N., Mestrot, A., Norton, G.J., Deacon, C.M., Meharg, A.A., 2012. Spatial heterogeneity and kinetic regulation of arsenic dynamics in mangrove sediments: the Sundarbans, Bangladesh. Environ. Sci. Technol. 46, 8645–8652. https://doi.org/10.1021/es301328r.

Hu, S., Lu, J., Jing, C., 2012. A novel colorimetric method for field arsenic speciation analysis. J. Environ. Sci. (China) 24, 1341–1346. https://doi.org/10.1016/S1001-0742(11)60922-4.

Huang, X.L., Zhang, J.Z., 2006. Surfactant-sensitized malachite green method for trace determination of orthophosphate in aqueous solution. Anal. Chim. Acta 580, 55–67. https://doi.org/10.1016/j.aca.2006.07.046.

Jeroschewski, P., Steuckart, C., Kühl, M., 1996. An amperometric microsensor for the determination of H2S in aquatic environments. Anal. Chem. 68, 4351–4357. https://doi.org/10.1021/ac960091b.

Kearns, J., Krupp, A., Hartman, S., Szogas, K., De Boskey, M., Harrington, J.M., 2019. Evaluation of arsenic field test kits as a learning exercise for engineering students in global water and sanitation class. Int. J. Serv. Learn. Eng. Humanit. Eng. Soc. Entrep. 14, 32–46. https://doi.org/10.24908/ijsle.v14i1.12528.

Klatt, J.M., Meyer, S., Häusler, S., Macalady, J.L., de Beer, D., Polerecky, L., 2016. Structure and function of natural sulphide-oxidizing microbial mats under dynamic input of light and chemical energy. ISME J. 10, 921–933. https://doi.org/10.1038/ismej.2015.167.

Kuramata, M., Abe, T., Matsumoto, S., Ishikawa, S., 2011. Arsenic accumulation and speciation in japanese paddy rice cultivars. Soil Sci. Plant Nutr. 57, 248–258. https://doi.org/10.1080/00380768.2011.565479.

Le, X.C., Yalcin, S., Ma, M., 2000. Speciation of submicrogram per liter levels of arsenic in water: on-site species separation integrated with sample collection. Environ. Sci. Technol. 34, 2342–2347. https://doi.org/10.1021/es991203u.

Lenoble, V., Deluchat, V., Serpaud, B., Bollinger, J.C., 2003. Arsenite oxidation and arsenate determination by the molybdene blue method. Talanta 61, 267–276. https://doi.org/10.1016/S0039-9140(03)00274-1.

Linge, K.L., Oldham, C.E., 2001. Interference from arsenate when determining phosphate by the malachite green spectrophotometric method. Anal. Chim. Acta 450, 247–252. https://doi.org/10.1016/S0003-2670(01)01388-5.

Lopez-Adams, R., Newsome, L., Moore, K.L., Lyon, I.C., Lloyd, J.R., 2021. Dissimilatory Fe(III) reduction controls on arsenic mobilization: a combined biogeochemical and NanoSIMS imaging approach. Front. Microbiol. 12, 219. https://doi.org/10.3389/FMICB.2021.640734/BIBTEX.

Mazumder, P., Sharma, S.K., Taki, K., Kalamdhad, A.S., Kumar, M., 2020. Microbes involved in arsenic mobilization and respiration: a review on isolation, identification, isolates and implications. Environ. Geochem. Health https://doi.org/10.1007/s10653-020-00549-8.

Mukherjee, A., Gupta, S., Coomar, P., Fryar, A.E., Guillot, S., Verma, S., Bhattacharya, P., Bundschuh, J., Charlet, L., 2019. Plate tectonics influence on geogenic arsenic cycling: from primary sources to global groundwater enrichment. Sci. Total Environ. 683, 793–807. https://doi.org/10.1016/j.scitotenv.2019.04.255.

Murphy, J., Riley, J.P., 1962. A modified single solution method for the determination of phosphate in natural waters. Anal. Chim. Acta 27, 31–36. https://doi.org/10.1016/S0003-2670(00)88444-5.

Nagul, E.A., McKelvie, I.D., Worsfold, P., Kolev, S.D., 2015. The molybdenum blue reaction for the determination of orthophosphate revisited: opening the black box. Anal. Chim. Acta 890, 60–82. https://doi.org/10.1016/j.aca.2015.07.030.

Nicholas, D.R., Ramamoorthy, S., Palace, V., Spring, S., Moore, J.N., Rosenzweig, R.F., 2003. Biogeochemical transformations of arsenic in circumneutral freshwater sediments. Biodegradation https://doi.org/10.1023/A:1024031700533.

Nickson, R., McArthur, J., Burgess, W., Matin Ahmed, K., Ravenscroft, P., Rahman, M., 1998. Arsenic poisoning of Bangladesh groundwater [7]. Nature https://doi.org/10.1038/26387.

Oremland, R.S., Stolz, J.F., 2003. The ecology of arsenic. Science (80-.) 300, 939–944. https://doi.org/10.1126/science.1081903.

Pett, L.B., 1933. The determination of inorganic phosphate in the presence of arsenic. Biochem. J. 27, 1672–1676. https://doi.org/10.1042/bj0271672.

Revsbech, N.P., 1989. An oxygen microsensor with a guard cathode. Limnol. Oceanogr. https://doi.org/10.4319/lo.1989.34.2.0474.

Richter, C., 2018. Spurensuche in Sachsen-Anhalt - Wie kommen Arsen und Cadmium in den Hamburger Hafen? Deutschlandfunk Kult.

Rodriǵuez-Lado, L., Sun, G., Berg, M., Zhang, Q., Xue, H., Zheng, Q., Johnson, C.A., 2013. Groundwater arsenic contamination throughout China. Science (80-.) 341, 866–868. https://doi.org/10.1126/science.1237484.

Sanger, C.R., Black, O.F., 1907. The quantitative determination of arsenic by the gutzeit method. Proc. Am. Acad. Arts Sci. 43, 297. https://doi.org/10.2307/20022326.

Saunders, J.K., Fuchsman, C.A., McKay, C., Rocap, G., 2019. Complete arsenic-based respiratory cycle in the marine microbial communities of pelagic oxygen-deficient zones. Proc. Natl. Acad. Sci. U. S. A. 116, 9925–9930. https://doi.org/10.1073/PNAS.1818349116/-/DCSUPPLEMENTAL.

Singh, K., Shukla, A.K., 2003. Poly-vinyl alcohol (PVA) and malachite green: a new reagent system for the microdetermination of phosphate in water and wastewater. Indian J. Environ. Health 45, 203–208.

Smedley, P.L., Kinniburgh, D.G., 2002. A review of the source, behaviour and distribution of arsenic in natural waters. Appl. Geochem. 17, 517–568. https://doi.org/10.1016/S0883-2927(02)00018-5.

Tapia, J., Murray, J., Ormachea, M., Tirado, N., Nordstrom, D.K., 2019. Origin, distribution, and geochemistry of arsenic in the altiplano-puna plateau of Argentina, Bolivia, Chile, and Perú. Sci. Total Environ. 678, 309–325. https://doi.org/10.1016/j.scitotenv.2019.04.084.

Thomas Arrigo, L.K., Mikutta, C., Lohmayer, R., Planer-Friedrich, B., Kretzschmar, R., 2016. Sulfidization of organic freshwater flocs from a minerotrophic peatland: speciation changes of iron, sulfur, and arsenic. Environ. Sci. Technol. 50, 3607–3616. https://doi.org/10.1021/acs.est.5b05791.

Van de Wiele, T., Gallawa, C.M., Kubachk, K.M., Creed, J.T., Basta, N., Dayton, E.A., Whitacre, S., Laing, G.Du., Bradham, K., 2010. Arsenic metabolism by human gut microbiota upon in vitro digestion of contaminated soils. Environ. Health Perspect. 118, 1004–1009. https://doi.org/10.1289/ehp.0901794.

Viollier, E., Inglett, P.W., Hunter, K., Roychoudhury, A.N., Cappellen, P.Van, 2000. The ferrozine method revisted. ApplGeochemistry 15, 785–790. https://doi.org/10.1016/S0883-2927(99)00097-9.

Wells, M., Kanmanii, N.J., Al Zadjali, A.M., Janecka, J.E., Basu, P., Oremland, R.S., Stolz, J.F., 2020. Methane, arsenic, selenium and the origins of the DMSO reductase family. Sci. Rep. 101 (10), 1–14. https://doi.org/10.1038/s41598-020-67892-9.

WHO, 2017. Guidelines for Drinking-water Quality. Fourth ed.

Williams, M., 2001. Arsenic in mine waters: an international study. Environ. Geol. 40.